EPJ Web of Conferences **75**, 05014 (2014)
DOI: 10.1051/epjconf/ 20147505014

Magnetotransport of indium antimonide doped with manganese

K. Kuzmina[1], B.A. Aronzon[1,2], A.V. Kochura[1,3], A.V. Lashkul[1], K.G. Lisunov[1,4], E. Lähderanta[1], and M.A. Shakhov[1,5]

[1]Department of Mathematics and Physics, Lappeenranta University of Technology, PO Box 20, FIN-53851 Lappeenranta, Finland
[2]P.N. Lebedev Physical Institute RAS, Leninskiy prospekt, 53, Moscow, Russia
[3]South-West State University, 50 let Oktjabrja Str., 305040 Kursk, Russia
[4]Institute of Applied Physics ASM, Academiei Str. 5, MD-2028 Kishinev, Moldova
[5]A.F. Ioffe Physico-Technical Institute, 194021 St. Petersburg, Russia

Abstract. Magnetotransport, including the magnetoresistance (MR) and the Hall effect, isinvestigated in polycrystalline $In_{1-x}Mn_xSb$ samples with $x = 0.02 – 0.06$, containing nanosize MnSb precipitates. The relative MR, $\Delta\rho/\rho$, is positive within the whole range of $B = 0 – 10$ T and $T \sim 20 – 300$ K. The Hall resistivity, ρ_H, exhibits a nonlinear dependence on B up to the room temperature.MR is interpreted with the two-band model, suggesting two types of holes with different concentration and mobility. In addition, analysis of ρ_H (B, T) is performed by taking into account both the normal and the anomalous contributions. The latter is attributable to the effect of MnSb nanoprecipitates, having the ferromagnetic Curie temperature well above 300 K.

1 Introduction

Interest to the group III-V Mn-doped diluted magnetic semiconductors (DMS) is connected mainly to their potential applicability in spintronics [1]. However, utilization of DMS in spintronic devices requires high values of the ferromagnetic (FM) Curie temperature, T_C. On the other hand, intrinsic limitations existing in homogeneous III-V DMS permit to obtain materials only with T_C lyingwell below the room temperature, as far as a carrier-mediated ferromagnetism is considered[2].An effective way to overcome such limitations is creation of inhomogeneous materials by alloying III-V DMS with FM compounds of the Mn-V group,havingT_C well above the room temperature, such as MnSb withT_C = 585 K [3].

This way has been realized recently by doping InSbwith Mnat a non-equilibrium preparation conditions (direct alloying of InSb, Mn and Sb, followed by a fast cooling of the melt) [4]. The resulting compound, with a nominal formula $In_{1-x}Mn_xSb$ and$x = 0.01 – 0.06$,is referred below simplyas InMnSb due to a complicated magnetic system and only a minority(~ 10 – 20 %) of substitutional Mn entering directly the InSb lattice. Two other magnetic components were found to be atomic-size Mn dimers and MnSb nanoparticles with sizes ~ 100 – 600 nm and volume fraction$\eta \sim 1 – 4$ %, which provided interesting magnetic properties of the material, including saturation of the magnetization$M$ (B) up to T = 300 K already above the fields of $B \sim 1 –2$ T [4].

Here are reported measurements of the magnetoresistance and the Hall effect in the same InMnSb samples as those investigated in Ref. 4 and their detailed quantitative analysis.

2 Results and discussion

2.1 Experimental results

Preparation and characterization of polycrystalline InMnSb samples with x = 0.02, 0.03 and 0.06 referred below as # 2, # 3 and # 4, respectively, is described in detail in Ref. 4. The magnetotransport measurements of the samples were performed using the standard six-point geometry in pulsed magnetic fields B up to 10 T at temperatures between T=16– 320 K.

The Hall resistivity, ρ_H, exhibits a non-linear dependence on$B$ up to room temperature (see top panel of figure 1). The typical behavior of the relative magnetoresistance (MR), $\Delta\rho/\rho \equiv [\rho(B) – \rho(0)]/\rho(0)$, is exhibited in the bottom panel of figure 1.

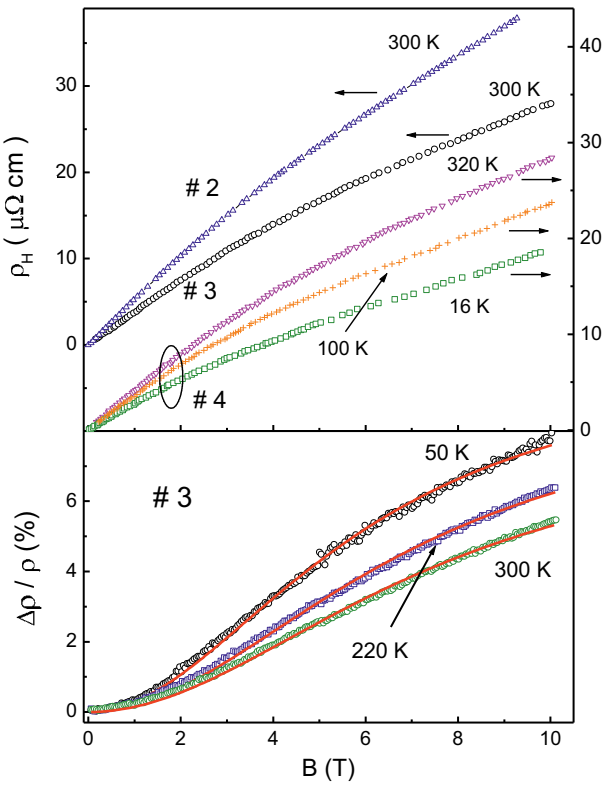

Fig. 1. The magnetic field dependences of ρ_H (top panel) and of$\Delta\rho/\rho$(bottom panel). The lines are calculated as described in the text.

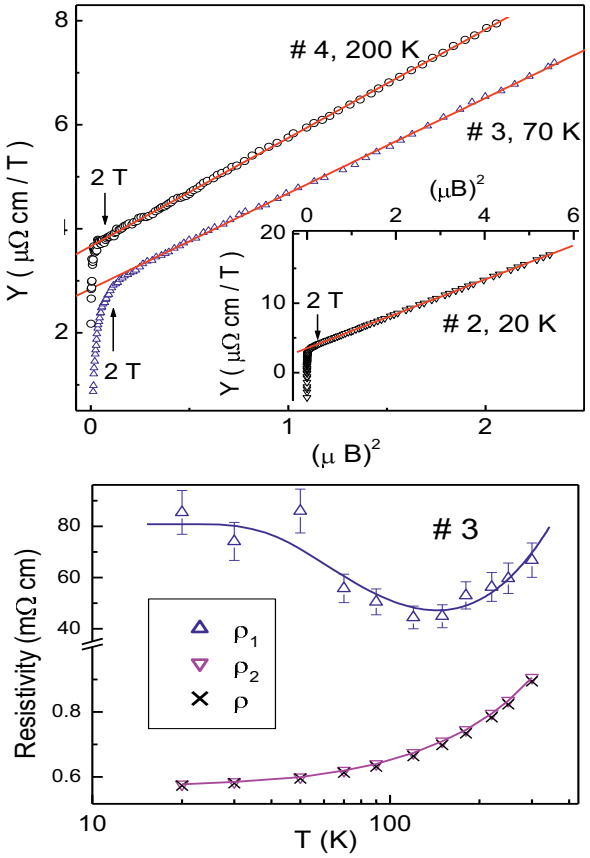

Fig. 2. The plots of Y vs. $(\mu B)^2$ (top panel) and the dependences ofρ_1,ρ_2 and ρ on T (bottom panel). The lines are linear fits (top panel) and guides for the eye (bottom panel).

2.2 Analysis of the results

In FM materials the Hall resistivity satisfies the expression

$$\rho_H(B) = R_N B + R_A M(B) \quad (1),$$

whereR_N and R_A are the normal and the anomalous Hall coefficients, respectively. The normal contribution to ρ_H is connected to the transverse electric field due to the Lorenz force, whereas the anomalous one to generation of the transverse electric field of another nature, governed by the influence of the spin-orbit interaction on the electron transport [5]. The latter is attributable to the effect of MnSb nanoprecipitates (see Introduction), which is one of the reasons to non-linearity of ρ_H (B) [4]. The second reason is possible contribution of two types of charge carriers with different concentration and mobility, addressed to the two-band model [6, 7]. In such conditions R_N becomes a function of B [7], which can be presented with the expression

$$R_N(B) = [R_0 + R_\infty(\mu B)^2] / [1 + (\mu B)^2]. \quad (2)$$

Here$R_0 = (R_1\rho_2^2 + R_2\rho_1^2)/(\rho_1 + \rho_2)^2$, $R_\infty = R_1R_2/(R_1 + R_2)$ and $\mu = (R_1 + R_2)/(\rho_1 + \rho_2)$are functions of R_j and ρ_j, where$j$ = 1 and 2 is the band number [8].Similar to Eq. (2), the resistivity in the two-band model can be expressed as [7, 8]

$$\rho(B) = [\rho_0 + \rho_\infty(\mu B)^2] / [1 + (\mu B)^2], \quad (3)$$

where$\rho_0 = \rho_1\rho_2/(\rho_1 + \rho_2)$ and $\rho_\infty = (\rho_2R_1^2 + \rho_1R_2^2)/(R_1^2 + R_2^2)$ [8]. If neither ofρ_j and R_j depends on B, then $\rho_0 = \rho(T)$ at B = 0 [7, 8] and MR in figure 1 can be fitted with Eq. (3)takingμ, ρ_0 and ρ_∞ independent of B,yielding the values of μ and ρ_∞. The plots of $\Delta\rho/\rho$ vs. B (lines in the bottom panel of figure 1), evaluated with Eq. (3) using the dependences of ρ (T) in zero field (not shown), exhibit a good agreement with the experimental data. Hence, the two-band model used above provides a reasonable explanation of positive MR in the investigated material.

Because $M(B)$ saturates already atB_S~ 1 – 2 T [4], for $B>B_S$ one can put $M\approx M_S=M$ (B_S) = const. Then, combining Eq. (1) and (2) one finds the expression

$$Y\equiv[\rho_H(B) - R_A M_S][1 + (\mu B^2)]/B = R_0 + R_\infty(\mu B)^2, \quad (4)$$

which suggests that Y is a linear function of $(\mu B)^2$for a correctly chosen value of R_AM_S. Such $R_AM_S$value can be obtainedunder condition of the best linearity of the plots

of Y vs. $(\mu B)^2$.This is achieved for all samples within the whole interval of T and between $B \sim 2 - 10$ T (examples are shown in the top panel of figure 2). Eventually, the linear fit of the obtained plots of Y vs. $(\mu B)^2$ yields the values of R_0 and R_∞, where the data of μ (T), obtained from the analysis of MR aboveand shown in the middle panel of figure 3,have been used.

With the expressions of R_0, R_∞, ρ_0, ρ_∞ and μ listedbelow Eq. (2) and (3), the values of $\rho_j$the Hall concentrations $p_j = (eR_j)^{-1}$ and the mobilities μ_j (j = 1 and 2), as well as those of$R_A M_S$ are evaluated. The dependences of these parameters on T for # 3 are displayed in the bottom panel of figure 2 and in the top, middle and bottom panel of figure 3, respectively.

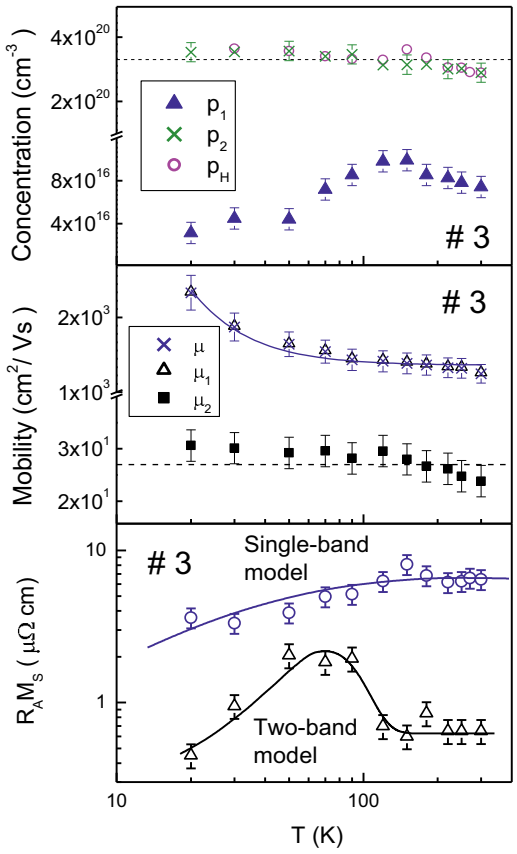

Fig. 3. Temperature dependences of p_1, p_2 andp_H (top panel), ofμ_1,μ_2 andμ(middle panel) and of $R_A M_S$(bottom panel) in # 3. The linesare to guide the eye.

Temperature dependences of p_j, μ_j and $R_A M_S$ in other samples are similar to those shown in figure 3 for # 3. Therefore, these data are given at some selected temperatures. Namely, $p_2 \approx 2.3\times10^{20}$ and 3.3×10^{20} cm^{-3}, and $\mu_2 \approx 35$ and 32 cm^2 /Vs for # 2 and # 4, respectively, exhibit no significant dependence on T within the error. In # 2 the values of $p_1 \approx$ 2.5, 7.5 and 6.6 (in units of 10^{16} cm^{-3}), μ_1 = 2500, 1600 and 1470 cm^2/Vs, and $R_A M_S \approx$6.5, 17 and 2.7μΩ cm at T = 20, 90 and 270 K, respectively, are obtained. Those in # 4 are as follows: $p_1 \approx$ 3, 8.6 and 9.7 (in units of 10^{16} cm^{-3}), $\mu_1 \approx$ 3060, 1600, 1320 cm^2/Vs and $R_A M_S \approx$ 3.5, 16.5 and 7.5 μΩ cm at T = 16, 100 and 320 K, respectively. Eventually, the relations of $\rho_1 >> \rho_2$ and $\rho_2 \approx \rho$ observed in # 3 (bottom panel of figure 3) are fulfilled in # 2 and # 4, as well.

Finally, as can be seen in the top panel of figure 1,the dependences of ρ_H (B) tends to linear functions above $B \sim$ 5 T. Therefore, the analysis of the Hall resistivity can be performed already within a single-band approximation, as made often in literature (see e. g. Refs. 6, 9-11). Namely, at B > 5 TM (B) is already saturated [4], which permits determination of R_N and $R_A M_S$ (both independent of B) by linear fits of ρ_H (B) in the high-field limit [11]. This yields the data of $p_H = (eR_N)^{-1}$ and $R_A M_S$ exhibited for # 3 in the top and bottom panels of figure 3, respectively.In other samples, the behavior of p_H and $R_A M_S$in the single-band approximation is similar to that in figure 3.

2.3Discussion

As follows from the results above, the two-band model permits interpretation of the positive MR and the Hall effect in the investigated InMnSb samples simultaneously, provided that all the partial contributions of ρ_j and R_j (j = 1 and 2) do not depend on the magnetic field [7]. Such supposition is well supported by the good agreement between the experimental (symbols) and the calculated (lines) dependences of $\Delta\rho/\rho$ on B(see the bottom panel of figure 1). Additional support is given by thebroad linear intervals on the plots of Y vs. $(\mu B)^2$, which is evident in the top panel of figure 2. The obtained relations of$\mu_1 >> \mu_2$ and $p_1 << p_2$ permits us to attribute the bands 1 and 2 to the light-holeband and the heavy- hole band of InSb [12], respectively. Indeed, the ratios of $\mu_1/\mu_2 \sim 40 - 90$ (see figure 3 and text below it) are comparable with that of the heavy-hole (hh) and the light hole (lh) effective masses,$m_{hh}/m_{lh} \sim 30$ [12]. On the other hand, the strong inequality $p_1 << p_2$ is consistent with the same relation between the density of states, determined by the effective mass ratio, as well.

Another interpretation of the origin of two bands with quite different concentration and mobility of the holes has been proposed recently to analyse the positive MR in InMnSb [6]. Such interpretation is based on spin-splitting of a single *p-d* hybridized valence band due to the kinetic *p-d* exchange, leading to shifts of the spin-up and spin-down bands towards energies above and below the Fermi energy, respectively [6]. Therefore, such shifts can lead to different hole concentrations in the bands. However, the ratio of $\mu_1/\mu_2 \sim 40 - 90$ observed here already in zero magnetic field looks overestimated, if it isascribed to different scattering of carriers with different spin polarization [6, 13]. Indeed, in such a case the values of the ratio of μ_1/μ_2only up to ~ 4 – 5 have been predicted at B as high as 10 T[13].

As can be seen in the bottom panel of figure 2, the resistivity of the investigated InMnSb samples is governed only by the contribution of the holes of the

band 2 (presumably the heavy-hole band). At the same time, the analysis of the Hall effect within a single-band approximation yields the values of p_H, practically coinciding with those of p_2 (circles and crosses in the top panel of figure 3, respectively). In this sense, the two-band model analysis of the Hall effect, being much more complicated, seems to give no advantage with respect to the more simple one considering only a single type of charge carriers. However, both analyses can be performed only within a field interval, where the magnetization is saturated, to satisfy the condition of $R_A M \approx R_A M_S$ = const. As can be seen in the top panel of figure 2, the onset of the linear part on the plots of Y vs. $(\mu B)^2$ at $B \approx 2$ T is close to the onset of saturation of the magnetization, $B_S \sim 1 - 2$ T [4] (see Introduction). At the same time, the plots of ρ_H (B) tend to linearity only at $B > 5$ T being evidently higher than B_S. Such contradiction provides additional support to the benefit of the two-band model approach above.

At this point, the difference between the behaviours of the anomalous contribution to the Hall effect in the bottom panel of figure 3 is noticeable. Indeed, the temperature maximum of $R_A M_S$ following from the two-band model analysis is rather unusual, whereas no such a maximum appears within a single-band consideration. On the other hand, as discussed above the two-band model analysisis substantiated well enough to attribute the non-monotonic behavior of $R_A M_S$to intrinsic properties of the material.

Finally, we discuss briefly possible influence of the metallic FM MnSb nanoinclusions on the normal Hall contribution, taking into account the values of the resistivity [14] and the normal Hall constant [14, 15] of bulk MnSb, R_N (MnSb), being much smaller those of our samples. With the results of Refs. 16 and 17, it can be shown that the value of p_H* corrected to presence of a fraction $\eta << 1$ of MnSb precipitates, is connected to p_H with the expression

$$\frac{p_H^*}{p_H} \approx \frac{(1-3\eta)^2}{1+3\eta-9\eta(1-\eta)R_N(MnSb)/R_N}. \qquad (5)$$

With the values of R_N (MnSb) ~ 10^{-3}– 10^{-4} cm^3/C [14, 15] and the data of η in Ref. 4, one can find only a small reduction of the Hall concentration by ~ 10 – 20 %.

Conclusions

We have investigated the positive magnetoresistance and the Hall effect in InMnSb containing nanosize MnSb precipitates. Both effects are interpreted with the two-band model, suggesting contributions of two types of holes with different concentration and mobility.The values of p_j and μ_j addressed to each type of charge carriers are obtained, attributing them presumably to the light and heavy holes of InSb. In addition, the anomalous contribution to the Hall effect is observed up 300 K. This is attributable to the effect of FM MnSb nanoprecipitates, having T_C well above the room temperature.

Acknowledgments

This work was supported by the Ministry of Education and Science of the Russian Federation (grant No. 3.5536.2011) and by the Russian Foundation for Basic Research (grants No. 13-02-01105a and and 13-02-92694).

References

1. I. Žutić, J. Fabian, S. Das Sarma, Rev. Mod. Phys. **76**, 323 (2004).
2. T. Jungwirth, J. Konig, J. Sinova, A.H. MacDonald, Phys. Rev. B **66**, 012402 (2002).
3. W.J. Takei, D. E.Cox, G. Shirane, Phys. Rev.**129**, 2008 (1963).
4. A.V. Kochura, B.A. Aronzon, K.G. Lisunov, A.V. Lashkul, A.A. Sidorenko, R. De Renzi, S.F. Marenkin, M. Alam, A.P. Kuzmenko, E Lähderanta, J. Appl. Phys. **113,** 083905 (2013).
5. L. Chien, C. Westgate, *The Hall effect and its applications* (Plenum, New York, 1980).
6. J.A. Peters, N.D. Parashar, N. Rangaraju, B.W. Wessels, Phys. Rev. **B** 82, 205207 (2010).
7. B.M. Askerov, *Electron Transport Phenomena in Semiconductors*(World Scientific, Singapore, 1994).
8. E.K. Arushanov, G.P. Chuiko, Phys. Status Solidi A **17**, K135 (1973).
9. R. Laiho, A.V. Lashkul, K.G. Lisunov, E. Lähderanta, M.A. Shakhov, V.S. Zakhvalinskii, Semicond. Sci. Technol **23**, 125001 (2008).
10. K. Ganesan, H. L. Bhatt, J. Appl. Phys. **103**, 043701 (2008).
11. S.V. Vonsovskii,*Magnetism* (Nauka, Moskow, 1971).
12. I. Vurgaftman, J.R. Meyer, L.R. Ram-Mohan, J. Appl. Phys. **89**, 5815 (2001).
13. M. Foygel, A.G. Petukhov, Phys. Rev. B **76**, 205202 (2007).
14. Tu Chen, W. Stutius, J. W. Allen, AIP Conf. Proc. **29**, 532 (1976).
15. M. Nogami, M. Sekinobu, H. Doi, Jpn. J. Appl. Phys. **3**, 572 (1964).
16. H. J. de Witt, J. Appl. Phys. **43**, 908 (1972).
17. M. Söderberg, G. Grimvall, J. Appl. Phys. **59**, 186 (1986).